Deletion of the Receptor for Advanced Glycation End Products Reduces Glomerulosclerosis and Preserves Renal Function in the Diabetic OVE26 Mouse

Nina Reiniger,[1] Kai Lau,[2] Daren McCalla,[1] Bonnie Eby,[2] Bin Cheng,[3] Yan Lu,[1] Wu Qu,[1] Nosirudeen Quadri,[1] Radha Ananthakrishnan,[1] Maryana Furmansky,[1] Rosa Rosario,[1] Fei Song,[1] Vivek Rai,[1] Alan Weinberg,[3] Richard Friedman,[4,5] Ravichandran Ramasamy,[1] Vivette D'Agati,[6] and Ann Marie Schmidt[1]

OBJECTIVE—Previous studies showed that genetic deletion or pharmacological blockade of the receptor for advanced glycation end products (RAGE) prevents the early structural changes in the glomerulus associated with diabetic nephropathy. To overcome limitations of mouse models that lack the progressive glomerulosclerosis observed in humans, we studied the contribution of RAGE to diabetic nephropathy in the OVE26 type 1 mouse, a model of progressive glomerulosclerosis and decline of renal function.

RESEARCH DESIGN AND METHODS—We bred OVE26 mice with homozygous RAGE knockout (RKO) mice and examined structural changes associated with diabetic nephropathy and used inulin clearance studies and albumin:creatinine measurements to assess renal function. Transcriptional changes in the Tgf-β1 and plasminogen activator inhibitor 1 gene products were measured to investigate mechanisms underlying accumulation of mesangial matrix in OVE26 mice.

RESULTS—Deletion of RAGE in OVE26 mice reduced nephromegaly, mesangial sclerosis, cast formation, glomerular basement membrane thickening, podocyte effacement, and albuminuria. The significant 29% reduction in glomerular filtration rate observed in OVE26 mice was completely prevented by deletion of RAGE. Increased transcription of the genes for plasminogen activator inhibitor 1, Tgf-β1, Tgf-β–induced, and α1-(IV) collagen observed in OVE26 renal cortex was significantly reduced in OVE26 RKO kidney cortex. ROCK1 activity was significantly lower in OVE26 RKO compared with OVE26 kidney cortex.

CONCLUSIONS—These data provide compelling evidence for critical roles for RAGE in the pathogenesis of diabetic nephropathy and suggest that strategies targeting RAGE in long-term diabetes may prevent loss of renal function. ***Diabetes*** **59: 2043–2054, 2010**

From the [1]Department of Surgery, Herbert Irving Comprehensive Cancer Center, Columbia University, New York, New York; the [2]Section of Nephrology, Department of Medicine, University of Oklahoma Health Sciences Center, Oklahoma City, Oklahoma; the [3]Department of Biostatistics, Herbert Irving Comprehensive Cancer Center, Columbia University, New York, New York; the [4]Department of Biomedical Informatics, Herbert Irving Comprehensive Cancer Center, Columbia University, New York, New York; the [5]Biomedical Informatics Shared Resource, Herbert Irving Comprehensive Cancer Center, Columbia University, New York, New York; and the [6]Department of Pathology, Herbert Irving Comprehensive Cancer Center, Columbia University, New York, New York.

Corresponding author: Nina Reiniger, nr2207@columbia.edu.

Received 2 December 2009 and accepted 4 May 2010. DOI: 10.2337/db09-1766.

The receptor for advanced glycation end products (RAGE), a member of the immunoglobulin superfamily, is upregulated in tissues subjected to the long-term impact of diabetes (1,2). The ligands of RAGE, including advanced glycation end products (AGEs), S100/calgranulins, and high mobility group box-1 (HMGB1) display elevated expression in diabetic tissues (1,2). In diabetic nephropathy, RAGE is upregulated in cells such as glomerular podocytes and endothelial cells in both humans and mice (2,3).

Previous studies provided evidence for roles for RAGE and its ligands in mouse models of early diabetic nephropathy. Overexpression of RAGE in vascular endothelial cells of hypo-insulinemic mice led to increased mesangial matrix expansion and glomerulosclerosis (4). Pharmacological blockade of RAGE, using the soluble extracellular ligand binding domain of RAGE (sRAGE), in type 2 insulin-resistant *db*/*db* diabetic mice, protected against glomerulosclerosis and other classical lesions of early diabetic nephropathy (3). In addition, the kidneys of streptozotocin-injected RAGE knockout (RKO) mice were protected from early mesangial matrix expansion and thickening of the glomerular basement membrane (GBM) seen in wild-type diabetic mice (3). Myint et al. (5) demonstrated protection from diabetic nephropathy in RKO mice crossed with transgenic mice expressing iNOS under the control of the insulin promoter. Others have shown that blocking antibodies to RAGE suppressed diabetic nephropathy in mouse models of type 1 and type 2 diabetes (6,7).

Until recently, very few mouse models of diabetic nephropathy progress beyond the early disease stages of microalbuminuria and mild mesangial expansion. Transgenic overexpression of calmodulin specifically in pancreatic β-cells, the OVE26 model of type 1 diabetes (8), resulted in nephromegaly, albuminuria, glomerulosclerosis, tubulointerstitial fibrosis, occasional occurrence of arteriolar hyalinosis, and the suggestion of decreased glomerular filtration rate (GFR) (9–11). Hence, the OVE26 mouse is considered one of the most human-relevant models of diabetic nephropathy studied to date.

We tested the hypothesis that RAGE contributes to advanced glomerulosclerosis and loss of renal function in long-term diabetes by crossing OVE26 mice with homozygous RAGE null mice to investigate the role of RAGE in this robust model of diabetic nephropathy.

RESEARCH DESIGN AND METHODS

Additional information is available in an online appendix at http://diabetes.diabetesjournals.org/cgi/content/full/db09-1766/DC1.

Mice. OVE26 mice [strain FVB(Cg)-Tg(Ins2-CALM1)26Ove Tg(Cryaa-TAg)1Ove/PneJ] and FVB controls (strain FVB/NJ) were obtained from The Jackson Laboratory (Bar Harbor, ME) and bred in house. FVB RKO mice, backcrossed over 10 generations into FVB, were bred in house and crossed with OVE26, resulting in OVE26 RKO mice. Changes associated with diabetic nephropathy were studied in male mice at 7 months based on our identification of this time point as one in which moderate to severe histologic renal changes are observed in most male OVE26 mice. Mice were killed at 1 month to test RAGE expression.

Polyclonal chicken anti-mouse RAGE IgY antibody production. Soluble (s)RAGE was produced as previously described (1). Anti-RAGE Chicken IgY was generated and purified from serum, and specificity for RAGE was confirmed.

Fluorescence microscopy. Frozen kidney sections were obtained from 1-month-old (for RAGE staining) and 7-month-old mice (for Glyoxalase1 [Glo1] staining) and stained with polyclonal chicken anti-mouse RAGE IgY or rat monoclonal (6F10) to Glo1 (Abcam, Cambridge, MA). Fluorescence microscopy was performed using a Lasersharp 2000 BioRad scanning confocal microscope (Bio-Rad, Hercules, CA).

Blood glucose and glycosylated hemoglobin measurements. Blood glucose measurements were taken in nonfasted mice at 4-week intervals and prior to killing at 7 months using a Freestyle blood glucose meter (Abbott, Alameda, CA). Levels above 499 mg/dl ("HI" reading), the maximum reading for the glucometer, were denoted as 500 mg/dl for calculation purposes. Blood hemoglobin A1C was measured using Cholestech GDX A1C test cartridges for human hemoglobin because the last 7 amino acids in the NH_2-terminus are identical between humans and mice (Cholestech, Harward, California).

Methylglyoxal measurement. Levels of methylglyoxal were determined in frozen kidney cortex tissue obtained from six female 7-month-old mice, as previously described (12).

Glyoxalase 1 Western. Kidney cortex lysate, 30 μg, was run on a 12% NuPAGE gel using MES running buffer (Invitrogen, Carlsbad, CA) under reducing conditions. After transfer to nitrocellulose membrane (Invitrogen), staining was performed using rat monoclonal (6F10) to Glo1 (1:1,000) (Abcam, Cambridge, MA) followed by chicken anti-rat antibodies (1:1,000) (Santa Cruz Biotechnology, Santa Cruz, Ca). Blots were then stripped with Restore Western Blot Stripping Buffer (Pierce, Rockford, IL) and probed with anti–β-actin antibody (1:2,500) (Becton Dickinson, Franklin Lakes, NJ). Bands were quantified using Alpha imaging software (Alpha Innotech, San Leandro, CA).

Morphometry. Kidneys were harvested and bisected longitudinally. One half kidney was fixed in 10% formalin overnight then dehydrated, embedded in paraffin, sectioned at 3 μm, mounted on 3-aminopropyltriethoxy silane–coated glass slides (Sigma, St. Louis, MO), stained with periodic acid Schiff (Sigma), and analyzed by light microscopy.

Pathology scoring. Pathology was scored in a semi-quantitative manner by a renal pathologist (V.D.'A.) blinded to the genotypes of the animals, as described in the online appendix.

GBM and podocyte effacement measurements. Glutaraldehyde fixed kidney cortex tissue was analyzed by electron microscopy. The thickness of the GBM of multiple capillaries was measured in 6–8 glomeruli per mouse ($n = 5$ per group). A mean of 55 measurements was taken per mouse (from podocyte to endothelial cell membranes) at random sites where the GBM was displayed in best cross-section. The same glomeruli were scored for degree of podocyte effacement, defined as the percentage of total glomerular capillary surface area over which the podocyte foot processes were effaced.

Urine collection and measurement of albuminuria. Urine was collected over 24 h from each mouse in individual mouse metabolic cages (Nalgene, Rochester, NY) and frozen at −80°C for subsequent analyses. Urinary albumin and creatinine levels were measured using the murine-specific Albuwell ELISA kit and the Creatinine Companion kit (Exocell, Philadelphia, PA) according to the manufacturer's instructions.

Measurement of GFR and effective renal plasma flow. Standard renal inulin clearance studies were performed during continuous hemodynamic monitoring, as published (13,14), in male mice at 7 months of age. Details are provided in the online appendix.

Glomerular isolation. Glomeruli were isolated by perfusing anesthetized mice with Dynabeads (Invitrogen), digesting the kidney tissue, and performing a series of sieving steps. Glomeruli were picked under the microscope using a pipette and placed in RNAlater (Ambion, Austin, TX).

RNA isolation, reverse transcription, and real time. RNA was isolated from ~20–30 mg of kidney cortex tissue (real-time for all, with the exception of Glo1) or ~1,000 isolated glomeruli (real-time for Glo1 and microarray sample preparation) per mouse using the RNaqueous kit (Ambion), and reverse transcription was performed with the Superscript III kit (Invitrogen) according to the manufacturers' instructions. Real-time primers and probes for murine 18s, Glo1, Tgfb1, Tgfbi, Serpine1, and α1-(IV) collagen were purchased from PE Applied Biosystems (Foster City, CA). Real-time PCR was performed with an ABI Prism 7900HT Sequence Detection System with TaqMan PCR Master Mix (PE Applied Biosystems).

ROCK1 activity assays. Activation of ROCK1 was evaluated on lysates of kidneys isolated from OVE26 or OVE26 RKO mice, as previously described (15). Details are provided in the online appendix.

Microarray experimental methods. RNA was isolated from ~1,000 isolated glomeruli per mouse using the RNaqueous kit (Ambion). Total RNA concentration was assessed using a ND-1000 NanoDrop Spectrophotometer (Thermo Scientific, Wilmington, DE), and quality was assessed on a 2100 Bioanalyzer system (Agilent Technologies, Santa Clara, CA) using the Agilent RNA 6000 Nano kit. The RNA was then amplified, and the biotin was labeled and fragmented using the Gene Chip 3'IVT Express Kit (Affymetrix, Santa Clara, CA). Fragmented RNA, 10 μg, was hybridized to Mouse Genome 430.2.0 GeneChips (Affymetrix). All samples were prepared with the two-cycle protocol recommended by the manufacturer. One array per mouse was used. Three arrays (mice) for each genotype were used.

Microarray data analysis. Microarray data was analyzed as described in the online appendix. All microarray data has been deposited in Gene Expression Omnibus (accession number GSE20844).

Statistical analysis. For the statistical analysis of all the datasets comparing the four groups, a one-way ANOVA model followed by paired comparisons was performed. Bonferroni correction due to multiple comparisons was used to control the overall type I error rate. Log transformation was used for the urine albumin-to-creatinine analysis (see Fig. 5). (For Fig. 3*D* and *E*, the comparison was done only between OVE26 and OVE26 RKO groups because the values for other groups were 0.) The severity of mesangial sclerosis data was compared using the Fisher exact test for contingency table (Fig 3*E*). All other data comparing two groups were analyzed using an independent two-sample *t*-test. Analyses were performed in SAS version 9.1 (SAS Institute, Cary, NC), with the exception of the ANOVA and *t*-tests, which were performed using Stat View (Adept Scientific, Acton, MA).

RESULTS

RAGE is expressed in glomeruli of OVE26 mice. Previous studies reported that RAGE is expressed in human and murine glomeruli (2), but expression had not been studied in the OVE26 model. RAGE was detected in the glomeruli of kidney cortex from male OVE26 mice at 1 month of age, and a baseline level of RAGE in the FVB glomerulus is provided for comparison (Fig. 1*A*). This time point was chosen to determine whether RAGE expression was present in the OVE26 mouse before observable structural changes in the kidney, thus correlating changes in RAGE with the timing of early stages of diabetic nephropathy development.

Precursor to RAGE ligands is reduced by RKO in OVE26 mice despite persistent hyperglycemia. OVE26 mice displayed significant increases in blood glucose levels compared with the nondiabetic FVB mice (498 ± 6 vs. 138 ± 36 mg/dl) ($P < 0.001$) (Fig. 1*B*). RKO did not alter the degree of hyperglycemia in OVE26 mice (494 ± 11 mg/dl) ($P = 0.7438$). Blood glucose levels measured at 4-week intervals beginning at 8 weeks of age showed the same trends among groups as the measurements at 7 months (data not shown).

A1C was significantly increased in OVE26 mice versus FVB controls (8.87 ± 0.33 vs. 5.35 ± 0.25%) ($P < 0.0001$) (Fig. 1*C*), confirming sustained hyperglycemia (Fig. 1*B*). A1C was normal in FVB mice, with or without RAGE (5.35 ± 0.25 vs. 6.03 ± 0.57%) (Fig. 1*C*). Importantly, A1C was comparably elevated among OVE26 mice with or without RAGE (8.87 ± 0.33 vs. 8.95 ± 0.41%) (Fig. 1*C*), confirming that RKO did not affect glycemic control.

We studied the effect of RAGE deletion in the context of hyperglycemia on the levels of methylglyoxal, a key precursor of AGEs. Levels of methylglyoxal were 3.25-fold higher in OVE26 kidney cortex compared with FVB ($P < 0.05$), but were unaffected by RKO in FVB mice. However, levels of methylglyoxal were 5.93-fold lower in OVE26 RKO cor-

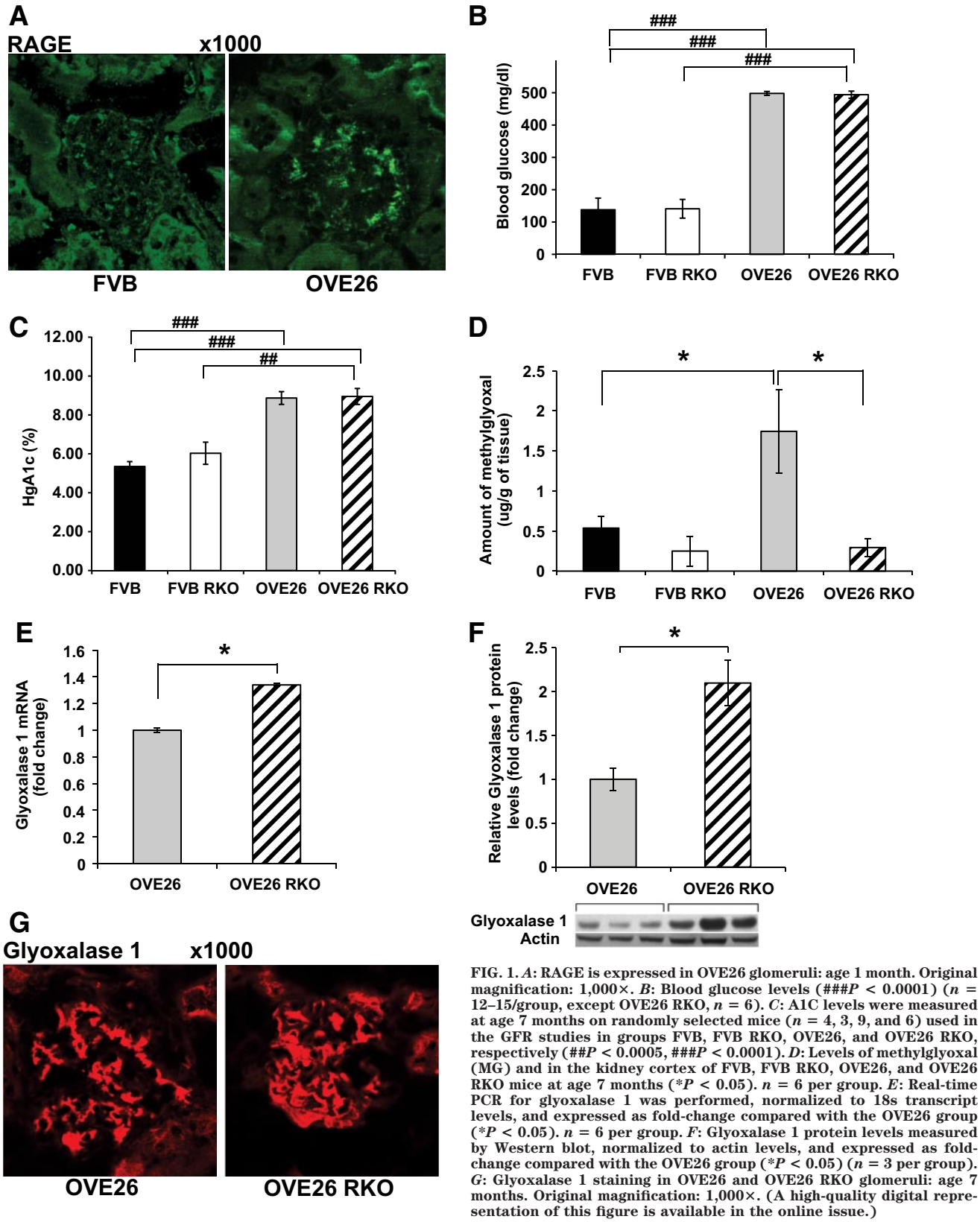

FIG. 1. *A*: RAGE is expressed in OVE26 glomeruli: age 1 month. Original magnification: 1,000×. *B*: Blood glucose levels (###$P < 0.0001$) (n = 12–15/group, except OVE26 RKO, $n = 6$). *C*: A1C levels were measured at age 7 months on randomly selected mice ($n = 4$, 3, 9, and 6) used in the GFR studies in groups FVB, FVB RKO, OVE26, and OVE26 RKO, respectively (##$P < 0.0005$, ###$P < 0.0001$). *D*: Levels of methylglyoxal (MG) and in the kidney cortex of FVB, FVB RKO, OVE26, and OVE26 RKO mice at age 7 months (*$P < 0.05$). $n = 6$ per group. *E*: Real-time PCR for glyoxalase 1 was performed, normalized to 18s transcript levels, and expressed as fold-change compared with the OVE26 group (*$P < 0.05$). $n = 6$ per group. *F*: Glyoxalase 1 protein levels measured by Western blot, normalized to actin levels, and expressed as fold-change compared with the OVE26 group (*$P < 0.05$) ($n = 3$ per group). *G*: Glyoxalase 1 staining in OVE26 and OVE26 RKO glomeruli: age 7 months. Original magnification: 1,000×. (A high-quality digital representation of this figure is available in the online issue.)

tex compared to OVE26 cortex ($P < 0.05$), despite equivalent degrees of hyperglycemia in both groups (Fig. 1*D*).

Glyoxalase 1 levels are increased by RKO in OVE26 mice. To further probe the differences in methylglyoxal levels among OVE26 and OVE26 RKO cortex, we assessed the levels of mRNA and protein for glyoxalase 1, an important regulator of methylglyoxal levels in vivo. Our data revealed that both mRNA transcript levels ($P < 0.05$) (Fig. 1*E*) and protein levels for glyoxalase 1 were higher in OVE26 RKO compared with OVE26 ($P < 0.05$) (Fig. 1*F*). Immunofluorescence staining localized glyoxalase 1, par-

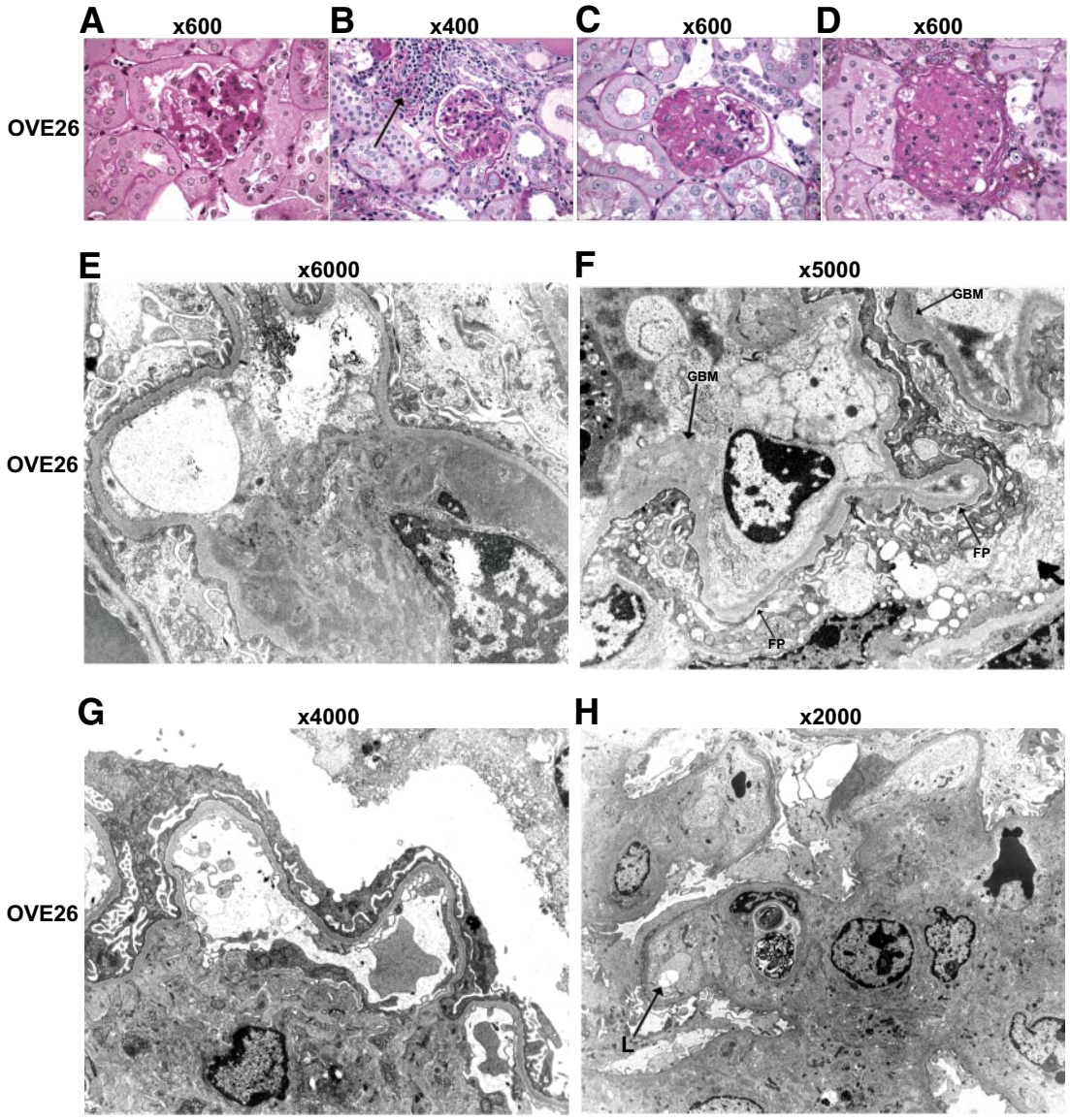

FIG. 2. Histology and ultrastructural pathology in diabetic OVE mice: age 7 months. By light microscopy, the glomeruli of 7-month-old male OVE26 mice display global mesangial sclerosis with nodularity (*A*), with progression in some glomeruli to segmental glomerulosclerosis (*C*) and global glomerulosclerosis (*D*). There is focal tubular atrophy, interstitial fibrosis, and chronic inflammation (*B*). By electron microscopy, the mesangial areas are expanded by increased matrix and electron dense hyaline material, consistent with insuded plasma proteins (*E*). There is thickening of glomerular basement membranes with overlying effacement of foot processes (*F*). Some mesangial areas have marked mesangial sclerosis with a nodular aspect (*G*). In areas of severe mesangial sclerosis, the glomerular capillary lumina are narrowed and focally occluded by the mesangial encroachment (*H*, L = lumen) (*arrow* indicates focal lumenal occlusion). Original magnifications are marked above each image. (A high-quality digital representation of this figure is available in the online issue.)

ticularly to the glomeruli of OVE26 and OVE26 RKO mice (Fig. 1*G*).

OVE26 RKO mice are partially protected from glomerulosclerosis. To establish the optimal time point for testing the role of RAGE in diabetic nephropathy in the OVE26 model in mice raised in our facility, we monitored the pathological changes in the kidney at 5, 6, and 7 months of age. At 5 months of age, mesangial sclerosis was mild in most OVE26 mice. At 6 months of age, more OVE26 mice revealed moderate pathology. At 7 months of age, we consistently observed a range of moderate to severe mesangial sclerosis including the formation of mesangial nodules causing capillary luminal narrowing (Fig. 2*A*), focal tubular atrophy, interstitial fibrosis and chronic inflammation (Fig. 2*B*), and progression to segmental (Fig. 2*C*) and global glomerulosclerosis (Fig. 2*D*). Glomeruli of OVE26 mice appeared enlarged compared with FVB controls (Fig. 3*A* and *B*), owing to diffuse and global mesangial sclerosis (Fig. 3*B*, *right panel*). The cortical tubules contained focal proteinaceous casts (Fig. 3*B*, *left panel*). Thus, to investigate the role of RAGE in advanced diabetic nephropathy, we studied OVE26 mice crossed with FVB RKO mice at age 7 months. OVE26 RKO mice were partially protected from these pathological alterations, including significantly fewer casts (Fig. 3*C* and *D*) and reduced mesangial matrix expansion (Fig. 3*C* and *E*) ($P < 0.05$). Tubular atrophy that was present in OVE26 mice (Fig. 2*B*) was completely prevented in OVE26 RKO mice (data not shown). The histology of FVB RKO mice did not differ significantly from that of FVB mice (data not shown).

At the ultrastructural level, the mesangial areas in OVE26 glomeruli were expanded by increased matrix and hyalinosis (Fig. 2*E*), in some cases obliterating

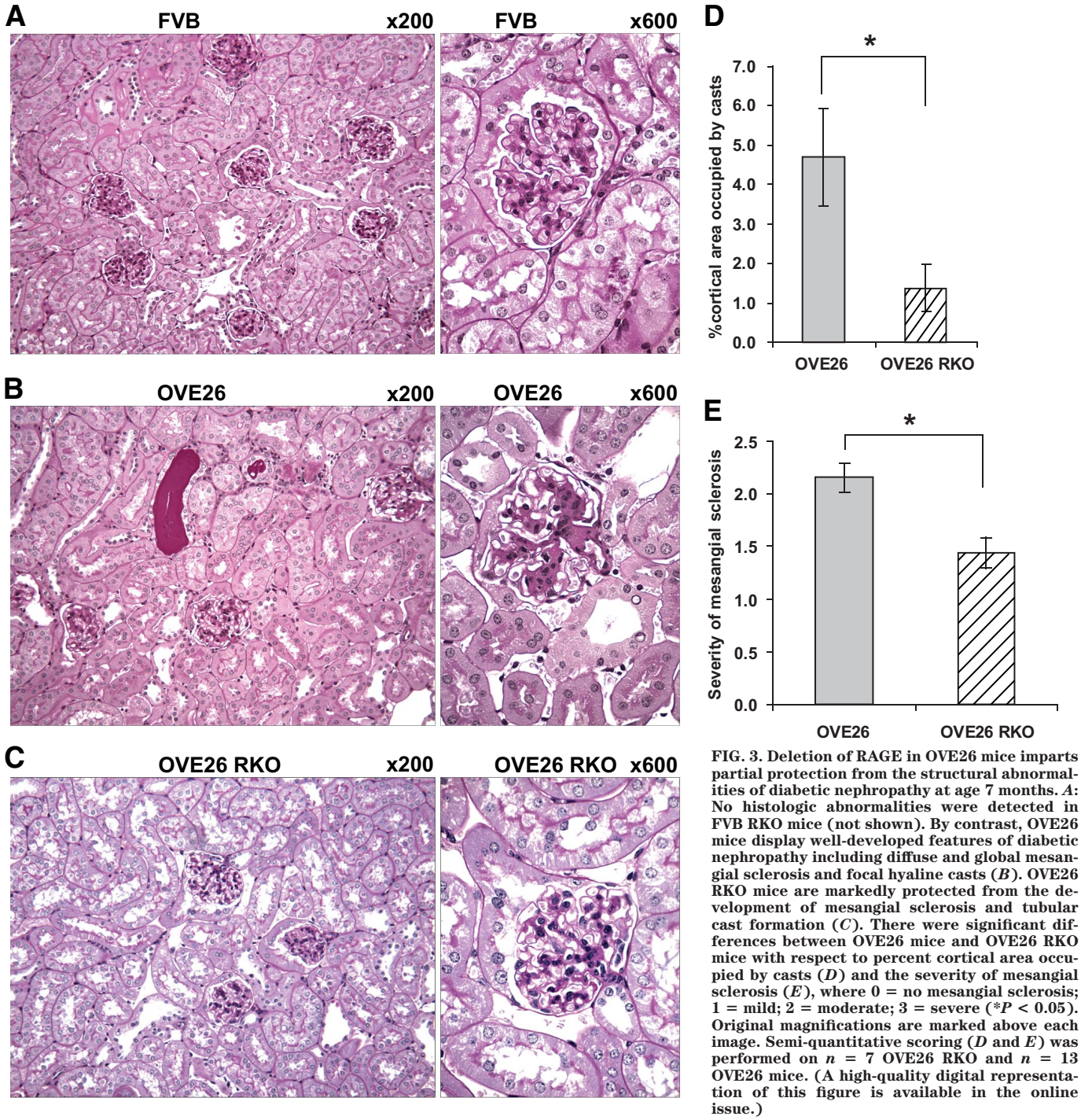

FIG. 3. Deletion of RAGE in OVE26 mice imparts partial protection from the structural abnormalities of diabetic nephropathy at age 7 months. *A*: No histologic abnormalities were detected in FVB RKO mice (not shown). By contrast, OVE26 mice display well-developed features of diabetic nephropathy including diffuse and global mesangial sclerosis and focal hyaline casts (*B*). OVE26 RKO mice are markedly protected from the development of mesangial sclerosis and tubular cast formation (*C*). There were significant differences between OVE26 mice and OVE26 RKO mice with respect to percent cortical area occupied by casts (*D*) and the severity of mesangial sclerosis (*E*), where 0 = no mesangial sclerosis; 1 = mild; 2 = moderate; 3 = severe (P* < 0.05). Original magnifications are marked above each image. Semi-quantitative scoring (*D* and *E*) was performed on *n* = 7 OVE26 RKO and *n* = 13 OVE26 mice. (A high-quality digital representation of this figure is available in the online issue.)**

capillary lumens (Fig. 2*H*). In OVE26 mice, the podocyte foot processes appeared effaced (Figs. 2*F–H* and 4*B*), and there was significant GBM thickening (Figs. 2*F* and 4*E*). In contrast, OVE26 RKO demonstrated less podocyte effacement than OVE26 (Fig. 4*C* and *D*) and no significant increase in GBM thickness compared with FVB mice (Fig. 4*C* and *E*) ($P < 0.05$). The glomeruli of FVB RKO mice were indistinguishable ultrastructurally from those of FVB mice (Fig. 4*D* and *E*, image not shown).

Albuminuria in OVE26 mice is markedly ameliorated by RKO. Urinary albumin and creatinine were measured at 7 months of age. OVE26 mice displayed significantly increased albumin-to-creatinine ratios compared to FVB mice (822 ± 159 vs. 46 ± 14 mg/mg) ($P < 0.001$) (Fig. 5). OVE26 RKO mice demonstrated significantly lower albumin-to-creatinine ratios (359 ± 152 mg/mg), reduced by ~56%, compared with OVE26 mice (Fig. 5) ($P = 0.0085$). FVB RKO albumin-to-creatinine ratios were not significantly different from FVB ratios ($P = 0.9793$).

Renal insufficiency is present in OVE26 mice but prevented by RKO

Metabolic, hematocrit, hemodynamic, and urine flow data in mice subjected to inulin clearance studies. Hematocrit (Hct) was comparable among the four groups, from the beginning to the end of the experi-

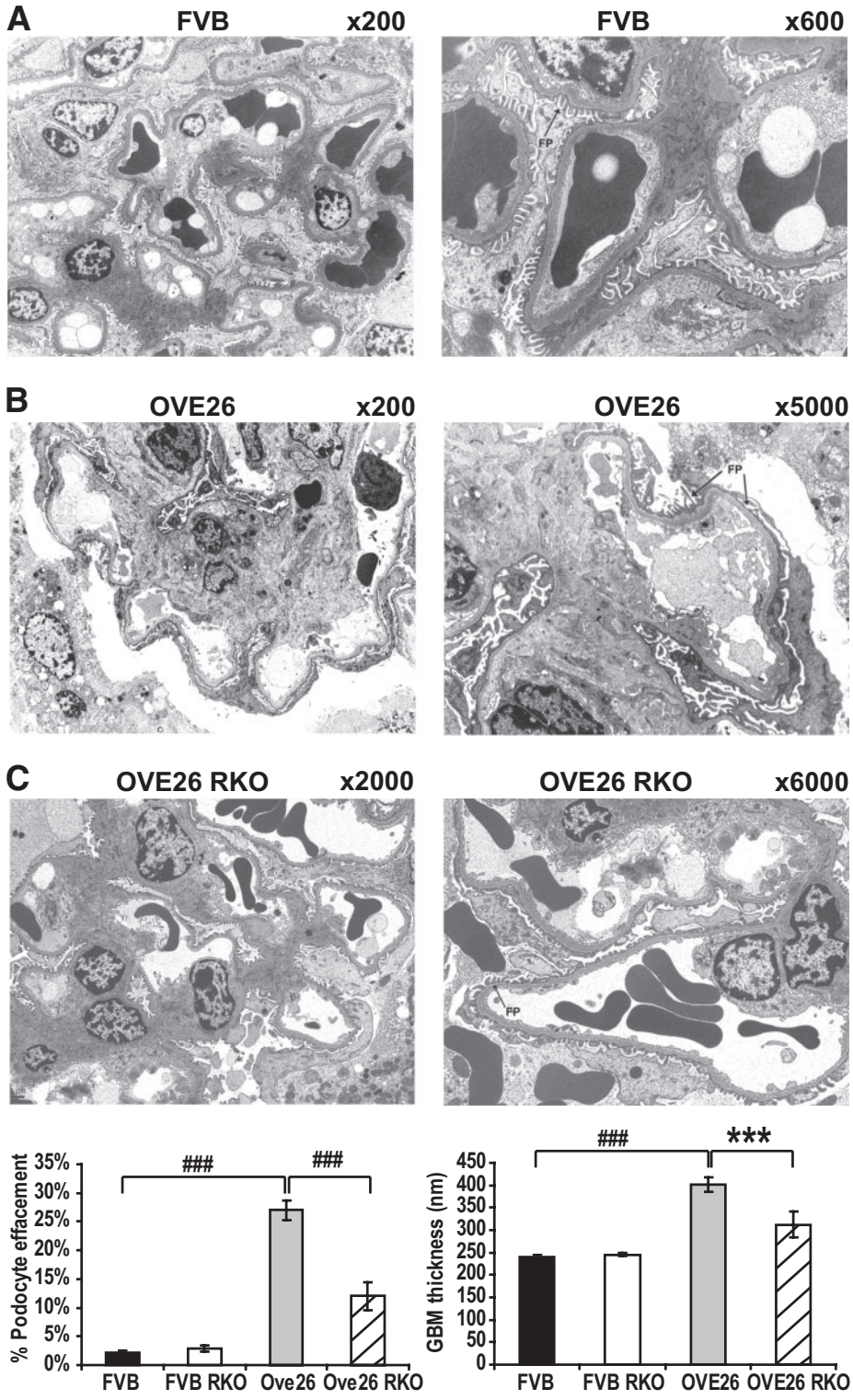

FIG. 4. Deletion of RAGE in OVE26 mice imparts partial protection from the ultrastructural abnormalities of diabetic nephropathy at age 7 months. Electron microscopy was performed on 7-month-old male kidney cortex samples. FVB mice display normal glomerular ultrastructural features with well-preserved foot processes and glomerular basement membranes of normal thickness (*A*). By comparison, OVE26 glomeruli display increased mesangial matrix forming focal nodules, thickened glomerular basement membranes, and prominent foot process effacement (*B*). OVE26 RKO mice were partially protected from these changes, leading to less mesangial sclerosis and partial restoration of foot processes (*C*). (*D*). Semi-quantitative scoring of podocyte effacement ($n = 5$) (*E*) Measurements of GBM thickness ($n = 5$) (*$P < 0.005$, ###$P < 0.0001$). Original magnifications are marked above each image.**

ment (Table 1), indicating negligible blood loss. In response to body weight–based mild saline infusion (to prevent volume depletion, especially in diabetic mice), all groups experienced a small but similar decline in Hct (Table 1). Throughout the 3-h experiment, Hct, averaged from five serial readings per mouse, was also comparable (Table 1), suggesting similar degrees of volume expansion and stability of blood volume. Mean systolic blood pres-

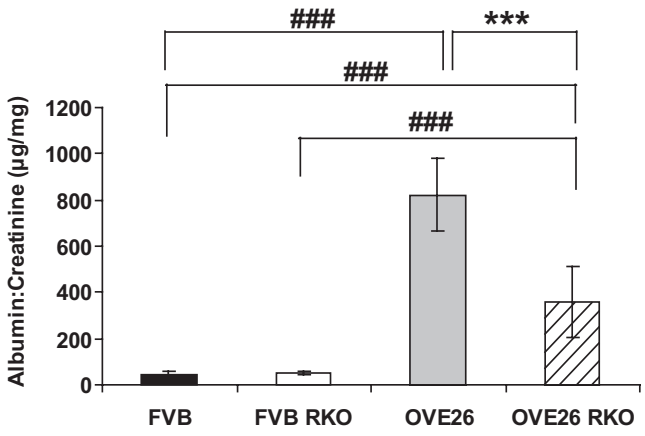

FIG. 5. Deletion of RAGE in OVE26 mice imparts partial protection from functional abnormalities of diabetic nephropathy at age 7 months. Albumin-to-creatinine levels were measured in male FVB, FVB RKO, OVE26, and OVE26 RKO mouse urine retrieved from metabolic cages at 7 months of age (*$P < 0.005$, ###$P < 0.0001$). n = 7–13 per group.**

sure was comparable among the four groups (Table 1), specifically without hypotension in any mice. Mean urine flow rates were similar between the FVB and OVE26 mice, without or with RKO (Table 1). Urine flow rate, however, was lower in the FVB RKO group versus the OVE26 RKO group ($P = 0.0073$). Despite this decrease in flow rate, their absolute urine volumes (>75 µl per period) posed no technical problems for counting inulin or quantification by mass. Overall, these hemodynamic parameters suggested good stability of the surgical preparations during anesthesia. Body weight (BW) was comparable among the four groups (Table 1). Weights of both kidneys (KW) in OVE26 mice were markedly increased (0.82 ± 0.03 vs. 0.49 ± 0.02 g in FVB controls, $P < 0.0001$) (Fig. 6*A*), consistent with the well-known nephromegaly in diabetes. Furthermore, KW/BW was also markedly increased in OVE26 versus FVB controls (2.82 ± 0.11 vs. 1.54 ± 0.08%, respectively; $P < 0.0001$) (Fig. 6*B*). Although nephromegaly was prominent in OVE26 diabetic mice, this was partially attenuated by RAGE deletion (0.71 ± 0.02 g, $P < 0.005$, $\Delta = 14\%$ reduction) (Fig. 6*A*). KW/BW of OVE26 mice was reduced by RKO (2.35 ± 0.05 vs. 2.82 ± 0.11%, $P < 0.001$, $\Delta = 17\%$ reduction) (Fig. 6*B*).

Absence of impaired renal functional phenotypes in FVB RKO mice. While RKO imparted major structural (Figs. 3 and 4) and functional effects in OVE26 mice (Figs. 5 and 6, vide infra), we could not detect any significant alterations in BW, Hct, systolic blood pressure, KW, or renal function in FVB RKO controls. More specifically, GFR was essentially unchanged by RKO in FVB mice whether expressed in units per mouse (Fig. 6*C*), per 100 g BW (Fig. 6*D*), or per grams KW (Fig. 6*E*).

Renal insufficiency in OVE26 versus nondiabetic controls. Compared with age- and sex-matched FVB controls, 7-month-old OVE26 mice showed a significant reduction in GFR (456 ± 18 vs. 325 ± 24 µl/min/mouse, $P < 0.0003$, $\Delta = 29\%$ reduction, Fig. 6*C*). The decline in GFR remained significant whether factored for BW (1,106 vs. 1,443 µl/min/100 g BW, $P < 0.003$, $\Delta = 24\%$ reduction, Fig. 6*D*) or factored for KW (401 vs. 940 µl/min/g KW, $P < 0.001$, $\Delta = 57\%$ reduction, Fig. 6*E*).

Preservation of renal function in OVE26 mice by RKO. In OVE26 mice, RKO prevented loss of GFR, which otherwise developed in OVE26 mice (436 ± 37 vs. 325 ± 24 µl/min per mouse, $P < 0.005$, $\Delta = 34\%$ increase, Fig. 6*C*). Further, in OVE26 mice, RKO preserved GFR, since levels were comparable to those of FVB and FVB RKO mice (456 ± 18 and 404 ± 21 µl/min per mouse, respectively; Fig. 6*C*). Likewise, reduction in renal function was prevented in OVE26 RKO mice versus OVE26 mice, whether GFR was factored by BW (1,457 ± 134 vs. 1,106 ± 78 µl/min/100 g BW, $P < 0.006$, $\Delta = 32\%$ increase, Fig. 6*D*) or factored by KW (620 ± 60 vs. 401 ± 35 µl/min/g KW, $P < 0.004$, $\Delta = 55\%$ increase, Fig. 6*E*). Significantly, in OVE26 RKO mice, GFR was preserved when factored for BW at levels similar to those of FVB controls, with or without RAGE (1,457 ± 134 vs. 1,443 ± 56 and 1,287 ± 64 µl/min/100 g BW, Fig. 6*D*). Although OVE26 RKO mice did not appear to have fully normalized GFR when factored by KW compared with levels of FVB controls (Fig. 6*E*), this was primarily a mathematical aberration and due to the marked nephromegaly (Fig. 6*A*). Although RKO significantly reduced KW of diabetic mice, the attenuation was only 14% (Fig. 6*A*). Thus, RKO is reno-protective in OVE26 mice. The prevention of renal insufficiency conferred by RKO is independent of glycemic control and systemic hemodynamic alterations.

Increases in PAI-1, Tgf-β1, Tgf-β–induced, and α1-(IV) collagen transcripts are found in OVE26 kidney cortex but are prevented by RAGE deletion. To explore the pathogenic mechanisms linked to diabetic nephropathy in OVE26 mice, we identified significant changes in *Serpine1* expression (the gene for plasminogen activator inhibitor 1 [PAI-1]) through a microarray study comparing expression of genes in isolated glomeruli from FVB and OVE26 mouse kidneys at 2 months of age. *Serpine1* levels were significantly increased by 1.46-fold in OVE26 glomeruli (false discovery rate = 0.02) (see supplemental Table S1 in the online appendix). To determine whether PAI-1 could be a downstream effector of RAGE in the diabetic kidney, we performed real-time PCR on kidney cortex RNA from mice at 7 months of age and found that levels of PAI-1 mRNA were increased 4.3-fold in OVE26 compared with FVB kidney cortex ($P < 0.0001$), whereas the levels in PAI-1 mRNA in OVE26 RKO were significantly lower

TABLE 1
Metabolic, hemodynamic, and urine flow data during inulin clearance studies

Groups	Genotypes		N	Body weight (g)	Hct initial (%)	Δ Hct (%)	Hct final (%)	Avg. of 5 Hct during clearance (%)	Avg. systolic BP (torr)	Avg. urine flow rate (µl/min)
I	FVB	Mean ± SE	10	31.65 ± 0.80	42.85 ± 1.10	−6.50 ± 0.78	36.38 ± 1.00	39.00 ± 1.10	109.37 ± 2.50	6.50 ± 1.19
II	FVB RKO	Mean ± SE	8	31.45 ± 0.85	44.06 ± 0.76	−5.11 ± 1.70	38.95 ± 2.15	40.19 ± 1.34	109.00 ± 3.43	4.11 ± 0.53
III	OVE26	Mean ± SE	9	29.30 ± 0.63	45.17 ± 1.71	−6.30 ± 1.71	38.90 ± 1.99	41.60 ± 1.30	105.61 ± 1.50	6.86 ± 0.61
IV	OVE26 RKO	Mean ± SE	6	30.16 ± 1.24	46.08 ± 1.57	−4.92 ± 1.72	41.20 ± 2.63	41.93 ± 2.00	107.80 ± 1.62	*9.08 ± 1.88

*$P < 0.01$ vs. group II.

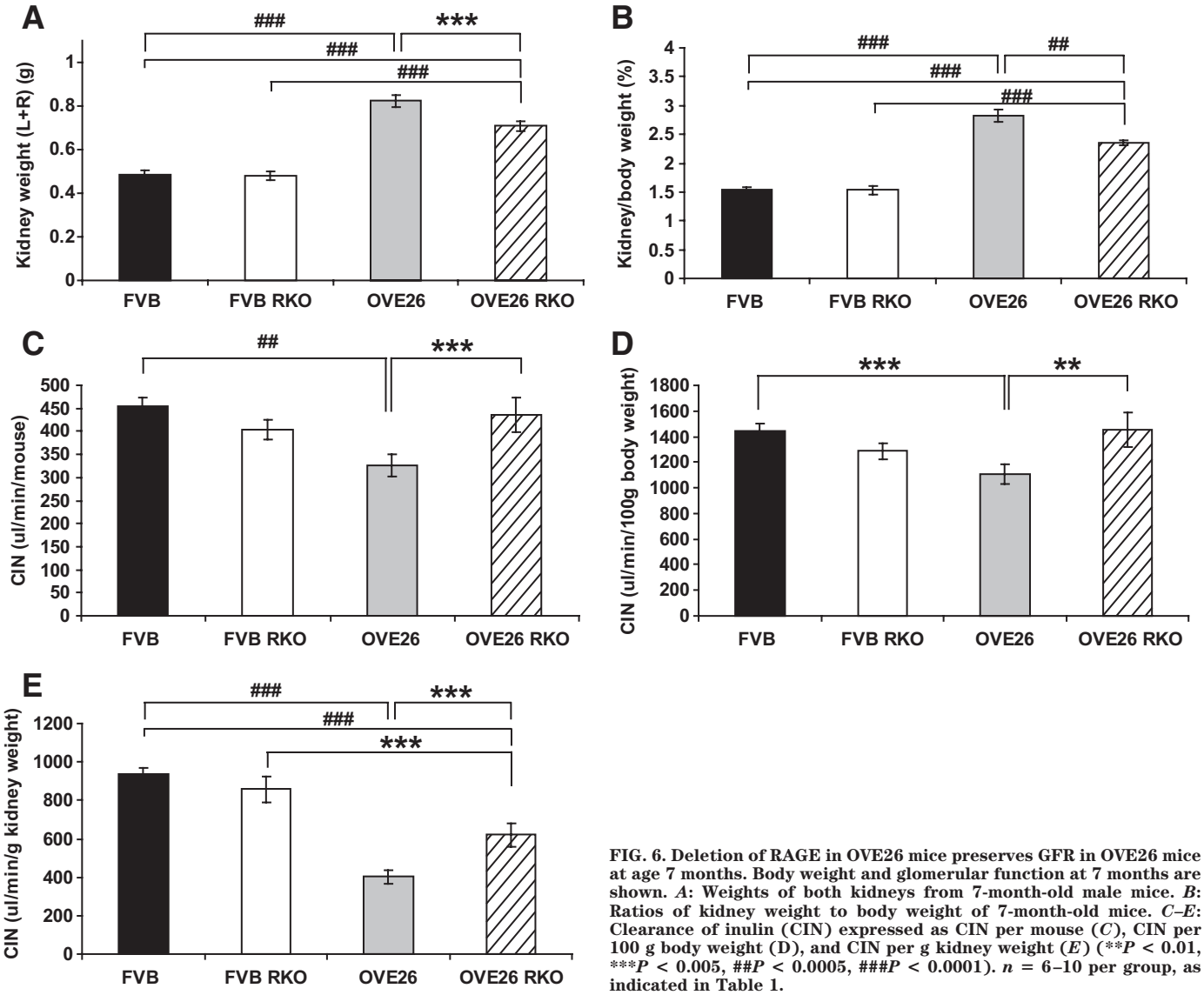

FIG. 6. Deletion of RAGE in OVE26 mice preserves GFR in OVE26 mice at age 7 months. Body weight and glomerular function at 7 months are shown. *A*: Weights of both kidneys from 7-month-old male mice. *B*: Ratios of kidney weight to body weight of 7-month-old mice. *C–E*: Clearance of inulin (CIN) expressed as CIN per mouse (*C*), CIN per 100 g body weight (D), and CIN per g kidney weight (*E*) ($P < 0.01$, ***$P < 0.005$, ##$P < 0.0005$, ###$P < 0.0001$). n = 6–10 per group, as indicated in Table 1.**

than those in OVE26 ($P < 0.0005$) and were not significantly different from FVB cortex ($P = 0.3723$) (Fig. 7*A*).

One of the central pathways that has been implicated in the pathogenesis of diabetic nephropathy is the Tgf-β pathway. Previous studies illustrated that PAI-1 expression may be induced by Tgf-β, leading to inhibition of extracellular matrix degradation (12–14). PAI-1 can also directly stimulate Tgf-β expression leading to increased synthesis of extracellular matrix (13). We thus performed real-time PCR on kidney cortex RNA from mice for *Tgf-b1* at 7 months of age and found that levels of *Tgf-b1* were increased 1.9-fold in OVE26 compared with FVB cortex ($P < 0.01$), whereas levels in OVE26 RKO were much lower and not significantly different from FVB cortex ($P = 0.8904$) (Fig. 7*B*).

To further investigate the impact of RAGE on the Tgf-β1 pathway in the OVE26 and OVE26 RKO cortex, we performed real-time PCR on *transforming growth factor (TGF)-β–induced* transcript as a measure of activity level and found significantly lower levels in OVE26 RKO compared with OVE26 cortex ($P < 0.0005$) (Fig. 7*C*).

In parallel, to explore the effects of RAGE on extracellular matrix deposition, we performed real-time PCR for *COL4A1*, the gene for α1-(IV) collagen, one of the collagen IV species secreted by podocytes of the glomeruli (15), and found significantly lower levels in OVE26 RKO compared with OVE26 cortex ($P < 0.001$) (Fig. 7*D*).

The type I Tgf-β receptor may interact with a number of different molecules including RhoA, which activates ROCK1 (16,17). ROCK1 has recently been shown to be potentially important in diabetic nephropathy (18,19) and has been shown to be downstream of RAGE signaling in the diabetic vasculature (20). We thus measured ROCK1 activity in OVE26 and OVE26 RKO kidney cortex and found that ROCK1 activity was significantly lower in OVE26 RKO compared with OVE26 cortex lysates ($n = 3$ per group) ($P < 0.005$) (Fig. 7*E*).

DISCUSSION

In this study, we used OVE26 mice to investigate the role of RAGE for the first time in a model displaying progressive and advanced features that closely resemble human diabetic nephropathy, including loss of GFR (10,11,21,22). Several previous models used to study RAGE, such as streptozotocin injection and *db/db* mice (3), do not progress beyond microalbuminuria and mild mesangial

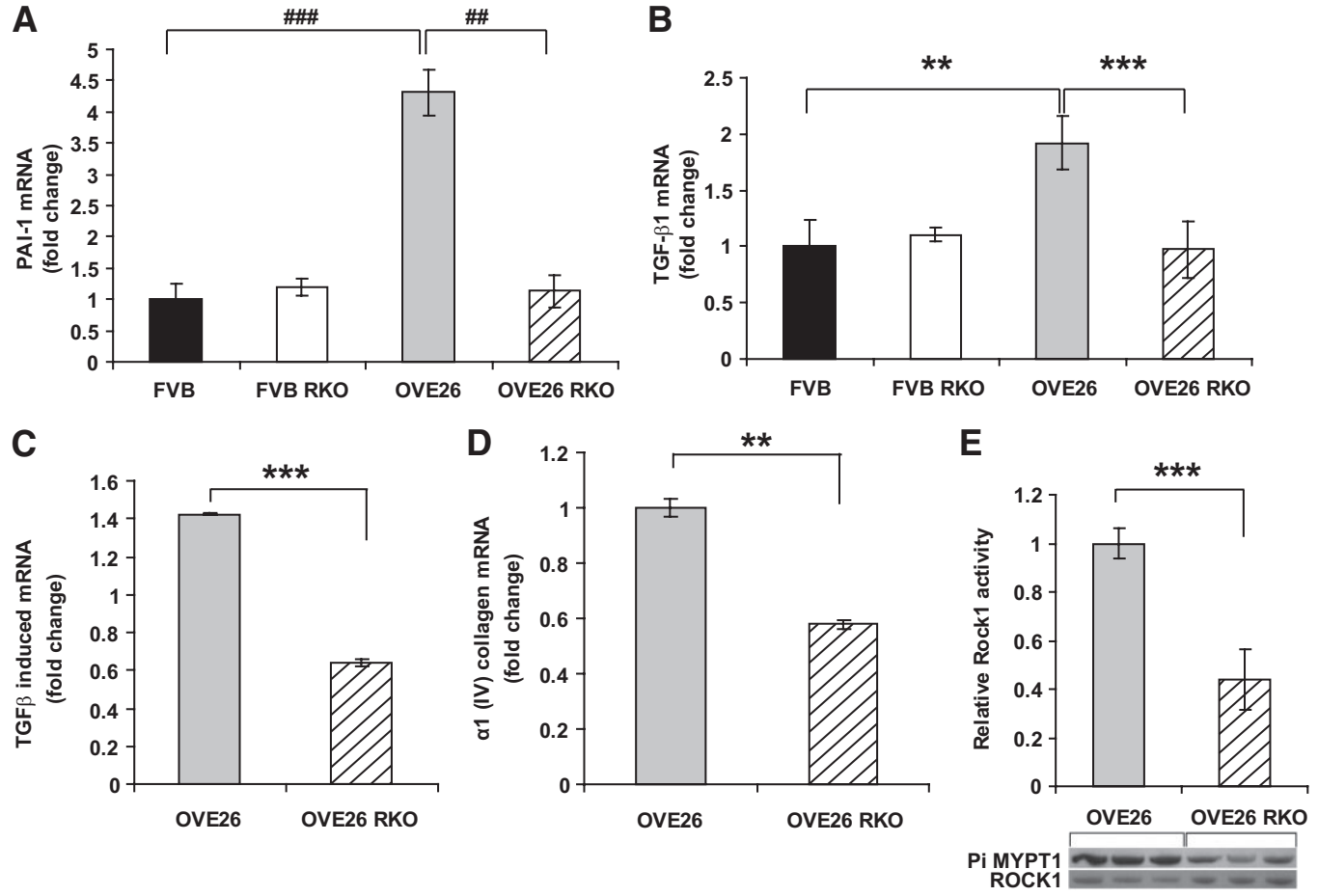

FIG. 7. PAI-1 (*Serpine1*), Tgf-β1, Tgf-β–induced, and α1-(IV) collagen mRNA transcripts and ROCK1 activity are lower in OVE26 RKO kidney cortex than in OVE26 kidney cortex levels at age 7 months. Real-time PCR for PAI-1 (*A*), Tgf-β1 (*B*), Tgf-β1–induced (*C*), and α1-(IV) collagen (*D*) gene products was performed, normalized to 18s transcript levels, and expressed as fold-change compared with the FVB or OVE26 group ($P < 0.01$, ***$P < 0.005$, ##$P < 0.0005$, ###$P < 0.0001$). $n = 6$ per group. *E*: ROCK1 activity was measured as the amount of phosphorylated MYPT1 compared with total ROCK1 levels by Western blot. Relative activity is expressed as fold-change compared with the OVE26 group (***$P < 0.005$) ($n = 3$ per group).**

expansion. Diabetic mice, due to the iNOS transgene, display advanced glomerulosclerosis but no tubulointerstitial fibrosis or arteriolar hyalinosis (4,23), features that are present in OVE26 mice (9).

Here, we have illustrated that several of these advanced features of diabetic nephropathy in the OVE26 model are affected by deletion of RAGE, such as the occurrence of segmental and global glomerular sclerosis, nodule formation, tubular atrophy, podocyte effacement, and thickening of the GBM. Importantly, the decline in GFR suggested previously in OVE26 mice, (9) and validated in our study, was completely prevented by RAGE deletion. In the previous study, however, although a 17% decrease in GFR in OVE26 versus nondiabetic control mice was demonstrated, this occurred in the presence of hypotension, thus supporting that the decline in GFR in OVE26 mice was due to the structural pathology associated with diabetic nephropathy and not hemodynamic factors (9).

A recent study reported increased serum creatinine in OVE26 mice but paradoxically increased creatinine clearance compared with FVB mice at ages 3, 6, and 9 months (11). This disparity underscores the limitations of using creatinine clearance to assess GFR, which could be inaccurate because of artifacts from urine collection or because of the use of non–high-performance liquid chromatography methods for determination of serum creatinine in diabetic animals (21,23,24). To overcome these limitations, we used inulin clearance, the gold standard for measuring GFR (25).

Beyond confirming previous findings of segmental and global sclerosis, nodule formation, and tubular atrophy, the observed decline in GFR in OVE26 mice in the absence of hypotension in our studies suggests a causal relationship with the pathology associated with diabetic nephropathy. This inference is supported by the degree of mesangial matrix expansion and the accompanying reduction in capillary lumen diameter, which would be expected to decrease ultrafiltration surface area and hence GFR. In addition, the focal tubular atrophy and interstitial fibrosis, which are known to correlate with declining renal function (26), may have contributed to renal insufficiency. This close functional-pathologic correlation helps establish the utility and validity of OVE26 mice to study clinical diabetic nephropathy, providing a basis to test the hypothesis of renoprotection by RKO.

Our results indicate that renal insufficiency in OVE26 mice was prevented by RKO, associated with significant ameliorations of pathology and albuminuria. Their nephromegaly was only minimally improved, possibly due to other upstream factors directly consequent to hyperglycemia. Over a shorter duration of streptozotocin-induced diabetes, we previously found normalization of KW/BW by

RKO (3). Another study found persistently increased glomerular volume despite marked podocyte loss in advanced diabetic nephropathy of OVE26 mice (22), making it conceivable for the coexistence of nephromegaly and preserved glomerular function.

Despite limitations of previously used diabetic nephropathy models, it has been reported that deletion or blockade of RAGE or inhibitors of AGE consistently led to partial preservation of renal structure and/or improved serum creatinine.(3,5–7,27–31) The diversity of these models provides further evidence for the role of RAGE, as sRAGE (3), anti-RAGE antibodies (6,7), or frank RAGE deletion exert salutary effects on the increased albuminuria and histopathology in early stages of mouse diabetic nephropathy. Previously, in 27-week-old *db*/*db* mice exhibiting low creatinine clearance, we found significant benefits of sRAGE administration (3), corroborating the adverse impact of RAGE on raising serum creatinine (4) and the salutary action by RKO on reducing serum creatinine in a type 1 diabetic nephropathy model (5). Our present studies, however, provide the first direct evidence for functional preservation in diabetic mice by RKO, as assessed by GFR.

Methylglyoxal, a highly reactive α-oxoaldehyde, is formed in cells primarily from the triose phosphate intermediates of glycolysis, dihydroxyacetone phosphate, and glyceraldehyde 3- phosphate. In diabetes, hyperglycemia triggers enhanced production of methylglyoxal, one consequence of which is the rapid modification of proteins and other substrates to generate AGEs, which may trigger signaling pathways leading to structural and functional changes of diabetic nephropathy, at least in part via the actions of TGF-β and PAI-1. The finding that methylglyoxal is significantly lower in OVE26 RKO mice, which have fewer structural changes and less functional impairment than OVE26 mice, supports this hypothesis. Notably, blood glucose levels in the OVE26 RKO did not differ significantly from the OVE26 mice. This suggests that the difference in levels of methylglyoxal did not result from a reduction in plasma glucose. Glyoxalase 1, a defense against glycation in vivo (32), detoxifies reactive α-oxoaldehydes, thereby removing deleterious species such as methylglyoxal. Our finding that glyoxalase 1 mRNA and protein levels are higher in OVE26 RKO mouse kidney cortex suggests that reduced activation of RAGE by AGEs may occur because of enhanced removal of methylglyoxal. The importance of the link between RAGE and glyoxalase 1 is that this may set up a positive feedback loop with relevant consequences. We have shown that by deleting RAGE, glyoxalase 1 mRNA and protein levels increase significantly, which decreases the tissue concentration of methylglyoxal and suppressed related AGE formation. These data suggest that disruption of RAGE signaling may be a beneficial therapeutic target in prevention of the progression of diabetic nephropathy.

To begin to explore potential molecular mechanisms accounting for the reduction in mesangial sclerosis noted in OVE26 RKO mice, we assessed mRNA levels of PAI-1, Tgf-β1, Tgf-β–induced, and α1-(IV) collagen. PAI-1 has been implicated previously in the pathogenesis of diabetic nephropathy. In PAI-1 knockout mice treated with streptozotocin or crossed with type 2 diabetic *db*/*db* mice, albuminuria was improved and glomerular injury was reduced compared with the diabetic PAI-1–expressing animals (13,33,34). A link between PAI-1 induction and RAGE has been previously demonstrated, but only in cell culture. Berrou et al. (35) measured PAI-1 protein expression in cultured mesangial cells in response to both glycated albumin and carboxymethyl lysine AGE, two RAGE ligands identified through in vitro experiments. An anti-RAGE antibody partially blocked the AGE and carboxymethyl lysine–induced PAI-1 expression in these cells. The significant reduction we find in Tgf-β1, Tgf-β–induced, and PAI-1 in OVE26 RKO mice suggests that deletion of RAGE may both reduce mesangial matrix accumulation and facilitate matrix degradation, both factors linked to reduced glomerulosclerosis. Reduced levels of α1-(IV) collagen expression in OVE26 RKO kidney cortex confirm these findings, since they are indicative of mesangial matrix accumulation.

Here we have shown that ROCK1 activity is significantly decreased in OVE26 RKO compared with OVE26 kidney cortex lysates. The importance of this finding is highlighted not only by known roles of R7OCK1 in diabetic nephropathy (18,19), the involvement of ROCK1 in Tgf-β, and PAI-1 downstream signaling (16,17), but also by our recent finding that activation of the ROCK1 branch of the Tgf-β pathway contributes to RAGE-dependent acceleration of atherosclerosis in diabetic ApoE null mice (20). The significant changes in ROCK1 activity in the kidney in the absence of RAGE suggests a novel mechanism by which RAGE may promote pathological change in diabetic nephropathy.

In future studies, exploration of the relevance of the OVE26 model of diabetic nephropathy to human diabetic nephropathy could be explored by administering renoprotective agents that are effective in humans, such as ACE inhibitors, to RAGE-expressing and RKO OVE26 mice. AGE formation and the renin-angiotensin system have been shown to interact in the progression of renal disease. Wilkinson-Berka et al. (36) have shown that blocking AGE formation can ameliorate angiotensin II–dependent renal injury. In addition, Thomas et al. (37) have shown that advanced glycation end products can activate ACE and other components of the intra-renal renin-angiotensin system. We have shown that increased levels of methylglyoxal are found in OVE26 kidney cortex and that the decreased pathology found in OVE26 RKO mice is accompanied by lower levels of methylglyoxal and increased glyoxalase 1 activity. We expect that treatment of OVE26 mice with ACE inhibitors could serve to prevent progression of renal disease in this model by potentially blocking ACE levels that may be elevated by the presence of excess AGEs in the OVE26 mice.

In conclusion, our data underscore important roles for RAGE in the structural and functional deteriorations in advanced and progressive diabetic nephropathy. Our findings support the notion that RAGE blockade may confer significant benefits by ameliorating severe renal histopathology and by preventing renal insufficiency in mice or patients at risk for diabetic nephropathy.

ACKNOWLEDGMENTS

This work was made possible with funding by the National Institutes of Health Ruth L. Kirschstein National Research Service Award 1F32DK076345-01 and the Juvenile Diabetes Research Foundation.

No potential conflicts of interest relevant to this article were reported.

N.R. prepared the initial main draft of the manuscript subsequently distributed to all coauthors for editing and

comments, substantial contribution to initial design of study, urine and tissue collection, blood glucose measurements, albumin and creatinine measurements, fluorescent staining imaging, glomerular isolation, RNA preparation, labeling and fragmentation of cDNA for microarray, real-time PCRs, breeding and maintenance of mouse colony, some statistical analysis excluding microarray, and coordination of mouse and mouse sample distribution to other coauthors; K.L. performed GFR, Hct, blood pressure, and A1C measurements, contributed to the manuscript, and reviewed and edited the manuscript; D.M. performed urine and tissue collection, blood glucose measurements, and albumin and creatinine measurements; B.E. provided GFR, Hct, blood pressure, and A1C measurements; B.C. carried out statistical analyses, excluding the microarray; Y.L. provided sections of frozen kidney tissue, fluorescent staining, and imaging; W.Q. generated the anti-RAGE antibody; N.Q. provided the methyl glyoxal measurements; R.A. contributed to the development and validation of the assays in the laboratory for the measurement of methylglyoxal, performed methyl glyoxal measurements, and reviewed and edited manuscript; M.F. performed tissue collection and glomerular isolation; R.R. performed breeding, genotyping, and maintenance of the mouse colony; F.S. performed breeding, genotyping, and maintenance of the mouse colony; V.R. provided the ROCK1 activity assay; A.W. provided statistical analyses, excluding the microarray; R.F. performed data analysis on the microarray results and reviewed and edited the manuscript; R.R. contributed to the initial design of the study, arranged funding, supervised research, developed and validated in the laboratory the assays for measurement of methylglyoxal, reviewed all primary data on measurements of methylglyoxal and glyoxalase 1, contributed to manuscript, and reviewed and edited the manuscript; V.D. performed analysis of the Periodic Acid Schiff-stained tissue sections and electron micrographs (including scoring of mesangial sclerosis, cast formation, GBM thickness measurements, and podocyte effacement), contributed to the initial design of the study, and reviewed and edited the manuscript; A.M.S. substantially contributed to the initial design of study, arranged funding, supervised research, reviewed all primary data with N.R. and determined the direction of the research, reviewed and edited the first draft of the manuscript prepared by N.R. before distribution to all coauthors, and reviewed and edited the manuscript.

Portions of this study were presented at the 2007, 2008, and 2009 annual meetings of the American Society of Nephrology.

The authors would like to thank Alexander Lau, University of Oklahoma, for help with the inulin clearance experiments and Joshua Karas, Columbia University, for help with mouse tissue collection and processing. In addition, the authors are grateful to Latoya Woods, Columbia University, for expert assistance in preparation of this manuscript.

REFERENCES

1. Park L, Raman KG, Lee KJ, Lu Y, Ferran LJ Jr, Chow WS, Stern D, Schmidt AM. Suppression of accelerated diabetic atherosclerosis by the soluble receptor for advanced glycation endproducts. Nat Med 1998;4:1025–1031
2. Tanji N, Markowitz GS, Fu C, Kislinger T, Taguchi A, Pischetsrieder M, Stern D, Schmidt AM, D'Agati VD. Expression of advanced glycation end products and their cellular receptor RAGE in diabetic nephropathy and nondiabetic renal disease. J Am Soc Nephrol 2000;11:1656–1666
3. Wendt TM, Tanji N, Guo J, Kislinger TR, Qu W, Lu Y, Bucciarelli LG, Rong LL, Moser B, Markowitz GS, Stein G, Bierhaus A, Liliensiek B, Arnold B, Nawroth PP, Stern DM, D'Agati VD, Schmidt AM. RAGE drives the development of glomerulosclerosis and implicates podocyte activation in the pathogenesis of diabetic nephropathy. Am J Pathol 2003;162:1123–1137
4. Yamamoto Y, Kato I, Doi T, Yonekura H, Ohashi S, Takeuchi M, Watanabe T, Yamagishi S, Sakurai S, Takasawa S, Okamoto H, Yamamoto H. Development and prevention of advanced diabetic nephropathy in RAGE-overexpressing mice. J Clin Invest 2001;108:261–268
5. Myint KM, Yamamoto Y, Doi T, Kato I, Harashima A, Yonekura H, Watanabe T, Shinohara H, Takeuchi M, Tsuneyama K, Hashimoto N, Asano M, Takasawa S, Okamoto H, Yamamoto H. RAGE control of diabetic nephropathy in a mouse model: effects of RAGE gene disruption and administration of low-molecular weight heparin. Diabetes 2006;55:2510–2522
6. Jensen LJ, Denner L, Schrijvers BF, Tilton RG, Rasch R, Flyvbjerg A. Renal effects of a neutralising RAGE-antibody in long-term streptozotocin-diabetic mice. J Endocrinol 2006;188:493–501
7. Flyvbjerg A, Denner L, Schrijvers BF, Tilton RG, Mogensen TH, Paludan SR, Rasch R. Long-term renal effects of a neutralizing RAGE antibody in obese type 2 diabetic mice. Diabetes 2004;53:166–172
8. Epstein PN, Overbeek PA, Means AR. Calmodulin-induced early-onset diabetes in transgenic mice. Cell 1989;58:1067–1073
9. Zheng S, Noonan WT, Metreveli NS, Coventry S, Kralik PM, Carlson EC, Epstein PN. Development of late-stage diabetic nephropathy in OVE26 diabetic mice. Diabetes 2004;53:3248–3257
10. Powell DW, Bertram CC, Cummins TD, Barati MT, Zheng S, Epstein PN, Klein JB. Renal tubulointerstitial fibrosis in OVE26 type 1 diabetic mice. Nephron Exp Nephrol 2009;111:e11–e19
11. Yuzawa Y, Niki I, Kosugi T, Maruyama S, Yoshida F, Takeda M, Tagawa Y, Kaneko Y, Kimura T, Kato N, Yamamoto J, Sato W, Nakagawa T, Matsuo S. Overexpression of calmodulin in pancreatic beta cells induces diabetic nephropathy. J Am Soc Nephrol 2008;19:1701–1711
12. Kutz SM, Hordines J, McKeown-Longo PJ, Higgins PJ. TGF-beta1-induced PAI-1 gene expression requires MEK activity and cell-to-substrate adhesion. J Cell Sci 2001;114:3905–3914
13. Nicholas SB, Aguiniga E, Ren Y, Kim J, Wong J, Govindarajan N, Noda M, Wang W, Kawano Y, Collins A, Hsueh WA. Plasminogen activator inhibitor-1 deficiency retards diabetic nephropathy. Kidney Int 2005;67:1297–1307
14. Baricos WH, Cortez SL, el-Dahr SS, Schnaper HW. ECM degradation by cultured human mesangial cells is mediated by a PA/plasmin/MMP-2 cascade. Kidney Int 1995;47:1039–1047
15. Iglesias-de la Cruz MC, Ziyadeh FN, Isono M, Kouahou M, Han DC, Kalluri R, Mundel P, Chen S. Effects of high glucose and TGF-beta1 on the expression of collagen IV and vascular endothelial growth factor in mouse podocytes. Kidney Int 2002;62:901–913
16. Mulder KM. Role of Ras and Mapks in TGFbeta signaling. Cytokine Growth Factor Rev 2000;11:23–35
17. Derynck R, Zhang YE. Smad-dependent and Smad-independent pathways in TGF-beta family signalling. Nature 2003;425:577–584
18. Peng F, Wu D, Gao B, Ingram AJ, Zhang B, Chorneyko K, McKenzie R, Krepinsky JC. RhoA/Rho-kinase contribute to the pathogenesis of diabetic renal disease. Diabetes 2008;57:1683–1692
19. Gojo A, Utsunomiya K, Taniguchi K, Yokota T, Ishizawa S, Kanazawa Y, Kurata H, Tajima N. The Rho-kinase inhibitor, fasudil, attenuates diabetic nephropathy in streptozotocin-induced diabetic rats. Eur J Pharmacol 2007;568:242–247
20. Bu DX, Rai V, Shen X, Rosario R, Lu Y, D'Agati V, Yan SF, Friedman RA, Nuglozeh E, Schmidt AM. Activation of the ROCK1 branch of the transforming growth factor-{beta} pathway contributes to RAGE-dependent acceleration of atherosclerosis in diabetic ApoE-null mice. Circ Res 2010;106:1040–1051
21. Breyer MD. Stacking the deck for drug discovery in diabetic nephropathy: in search of an animal model. J Am Soc Nephrol 2008;19:1623–1624
22. Teiken JM, Audettey JL, Laturnus DI, Zheng S, Epstein PN, Carlson EC. Podocyte loss in aging OVE26 diabetic mice. Anat Rec (Hoboken) 2008;291:114–121
23. Breyer MD, Böttinger E, Brosius FC 3rd, Coffman TM, Harris RC, Heilig CW, Sharma K, AMDCC. Mouse models of diabetic nephropathy. J Am Soc Nephrol 2005;16:27–45
24. Dunn SR, Qi Z, Bottinger EP, Breyer MD, Sharma K. Utility of endogenous creatinine clearance as a measure of renal function in mice. Kidney Int 2004;65:1959–1967
25. Gaspari F, Perico N, Remuzzi G. Measurement of glomerular filtration rate. Kidney Int Suppl 1997;63:S151–S154
26. Ziyadeh FN. The extracellular matrix in diabetic nephropathy. Am J Kidney Dis 1993;22:736–744
27. Miyoshi H, Taguchi T, Sugiura M, Takeuchi M, Yanagisawa K, Watanabe Y,

Miwa I, Makita Z, Koike T. Aminoguanidine pyridoxal adduct is superior to aminoguanidine for preventing diabetic nephropathy in mice. Horm Metab Res 2002;34:371–377
28. Peppa M, Brem H, Cai W, Zhang JG, Basgen J, Li Z, Vlassara H, Uribarri J. Prevention and reversal of diabetic nephropathy in db/db mice treated with alagebrium (ALT-711). Am J Nephrol 2006;26:430–436
29. Ellis EN, Good BH. Prevention of glomerular basement membrane thickening by aminoguanidine in experimental diabetes mellitus. Metabolism 1991;40:1016–1019
30. Soulis-Liparota T, Cooper M, Papazoglou D, Clarke B, Jerums G. Retardation by aminoguanidine of development of albuminuria, mesangial expansion, and tissue fluorescence in streptozocin-induced diabetic rat. Diabetes 1991;40:1328–1334
31. Vlassara H, Striker LJ, Teichberg S, Fuh H, Li YM, Steffes M. Advanced glycation end products induce glomerular sclerosis and albuminuria in normal rats. Proc Natl Acad Sci U S A 1994;91:11704–11708
32. Thornalley PJ. The glyoxalase system in health and disease. Mol Aspects Med 1993;14:287–371
33. Collins SJ, Alexander SL, Lopez-Guisa JM, Cai X, Maruvada R, Chua SC, Zhang G, Okamura DM, Matsuo S, Eddy AA. Plasminogen activator inhibitor-1 deficiency has renal benefits but some adverse systemic consequences in diabetic mice. Nephron Exp Nephrol 2006;104:e23–e34
34. Lassila M, Fukami K, Jandeleit-Dahm K, Semple T, Carmeliet P, Cooper ME, Kitching AR. Plasminogen activator inhibitor-1 production is pathogenetic in experimental murine diabetic renal disease. Diabetologia 2007; 50:1315–1326
35. Berrou J, Tostivint I, Verrecchia F, Berthier C, Boulanger E, Mauviel A, Marti HP, Wautier MP, Wautier JL, Rondeau E, Hertig A. Advanced glycation end products regulate extracellular matrix protein and protease expression by human glomerular mesangial cells. Int J Mol Med 2009;23:513–520
36. Wilkinson-Berka JL, Kelly DJ, Koerner SM, Jaworski K, Davis B, Thallas V, Cooper ME. ALT-946 and aminoguanidine, inhibitors of advanced glycation, improve severe nephropathy in the diabetic transgenic (mREN-2)27 rat. Diabetes 2002;51:3283–3289
37. Thomas MC, Tikellis C, Burns WM, Bialkowski K, Cao Z, Coughlan MT, Jandeleit-Dahm K, Cooper ME, Forbes JM. Interactions between renin angiotensin system and advanced glycation in the kidney. J Am Soc Nephrol 2005;16:2976–2984